International Journal of Plasticity 164 (2023) 103588

Contents lists available at ScienceDirect

International Journal of Plasticity

journal homepage: www.elsevier.com/locate/ijplas

Physics-motivated fractional viscoelasticity model for dynamic relaxation in amorphous solids

F. Zhu [a], G.H. Xing [a], G.J. Lyu [a], L.T. Zhang [a], Yun-Jiang Wang [b,c], Y. Yang [d,e], J. M. Pelletier [f], J.C. Qiao [a,*]

[a] School of Mechanics, Civil Engineering and Architecture, Northwestern Polytechnical University, Xi'an, 710072, China
[b] State Key Laboratory of Nonlinear Mechanics, Institute of Mechanics, Chinese Academy of Sciences, Beijing, 100190, China
[c] School of Engineering Science, University of Chinese Academy of Sciences, Beijing, 100049, China
[d] Department of Mechanical Engineering, College of Engineering, City University of Hong Kong, Tat Chee Avenue, Kowloon Tong, Kowloon, Hong Kong SAR, China
[e] Department of Materials Science and Engineering, College of Engineering, City University of Hong Kong, Tat Chee Avenue, Kowloon Tong, Kowloon, Hong Kong SAR, China
[f] Université de Lyon, MATEIS, UMR CNRS5510, Bat. B. Pascal, INSA-Lyon, F-69621 Villeurbanne Cedex, France

ARTICLE INFO

Keywords:
Non-Debye relaxation
Fractional derivative
Metallic glasses
Quasi-point defect
Structural heterogeneity

ABSTRACT

Dynamic mechanical relaxation is an important metric to understand the mechanical/physical properties of amorphous solids which are of viscoelastic nature. Due to the heterogenous microstructure, the relaxation behavior of amorphous solids usually shows strong deviation from the Debye relaxation. The distribution of relaxation time derived from either the stretched exponential function (KWW function) or the power law form is probably the most adopted paradigm to describe the non-Debye relaxation. They are essentially the continuous spectrums given in analytical forms. However, whether a real amorphous material conforms to such distribution law remains to be discussed. Here we test the assumption in typical metallic glasses (MGs) as representatives of the general amorphous solids. The mechanical spectrum of a $Cu_{46}Zr_{47}Al_7$ MG in wide frequency domain is probed by the dynamic mechanical analysis technique. It is found that both the KWW function and the modified fractional (MF) model based on power law can well describe the experimental data. As a step forward, we combine the quasi-point defect theory with the MF model to theoretically reveal the feature of temperature-dependent structural evolution in MG. Finally, the distribution of relaxation time corresponding to the experimental data is discretized to argue the theoretically predicted microstructural heterogeneity in the MGs.

1. Introduction

Amorphous solids, which are obtained from their supercooled liquids through glass transition, are characterized by the long-range structural disorder (Berthier and Biroli, 2011; Chen and Dai, 2016). Dynamic relaxation behavior exists ubiquitously in amorphous solids, and its internal mechanism is still elusive. α relaxation, as a common feature of the general amorphous materials, usually occurs near the glass transition temperature T_g and can be also observed in the mechanical relaxation and dielectric response (Cui et al.,

* Corresponding author.
E-mail address: qjczy@nwpu.edu.cn (J.C. Qiao).

https://doi.org/10.1016/j.ijplas.2023.103588
Received 22 November 2022; Received in revised form 26 February 2023;
Available online 5 March 2023

2017). By the energy landscape picture, α relaxation is explained as the transition between adjacent mega energy valleys, which are composed of many small energy valleys (Harmon et al., 2007). As a precursor of α relaxation, β relaxation is associated with the transition between these small energy valleys (Qiao et al., 2019). The energy landscape picture phenomenally describes the dynamic relaxation behaviors, which are derived from the disordered structure within amorphous solids. Therefore, a deep understanding of the dynamic relaxation mechanism is the key to deconstruct the intrinsic structure of amorphous solids.

Metallic glasses (MGs), as a kind of amorphous solids, are expected to be promising structural materials due to the excellent physical, chemical and mechanical properties (Ashby and Greer, 2006; Fu et al., 2020; Jiang et al., 2020; Sha et al., 2017; Wang, 2019; Qiao et al., 2022). Due to the disordered arrangement of atoms, there are no well recognized structural defects in analogy with those in the traditional crystalline alloys such as dislocations and grain boundaries (Hao et al., 2022; Qiao et al., 2019; Wang, 2012; Zhang et al., 2019). Compared with other amorphous solids (i.e., oxide glasses, amorphous polymers), MGs have relatively simple atomic structure and can be used as prototypical model for studying the microscopic mechanism of dynamic relaxation. Microstructural heterogeneity is an intrinsic structural feature of MGs, which should affect the distribution of relaxation time in MGs and further induces dynamic heterogeneity from a kinetic perspective (Kosiba et al., 2019; Tao et al., 2022; Duan et al., 2022). Therefore, dynamic relaxation behavior can be regarded as an important entry point to study the microstructural and dynamic heterogeneities in MGs.

The behavior of amorphous solids, in general, and of MGs in particular, depends very strongly on temperature and frequency. Dynamic mechanical analysis (DMA) has been widely used to study the dynamic relaxation behaviors of various MGs systems in a certain range of temperature and/or frequency (Cheng et al., 2021; Zhang et al., 2022). Many works have been carried out on modeling the viscoelastic response of MGs in both the temperature and frequency domains. The dynamic response can be described by the generalized Maxwell (GM) model or the generalized Kelvin–Voigt (GKV) model (Liu et al., 2022; Xu et al., 2022), however, these models always require a large number of fitting parameters which sometimes are lack of physical foundation. In order to avoid this limitation, traditional models, which are composed of spring and dashpot elements, are often abandoned and replaced by the empirical fitting functions. The Kohlrausch–Williams–Watts (KWW) function and Havriliak–Negami (HN) function, as the two most commonly used empirical fitting functions, have been proved to be able to describe the dynamic relaxation behaviors of MGs (Yao et al., 2017). Wang et al. (2014) associate the fitting parameter β_{KWW} (or β) of KWW function with the dynamic heterogeneity of supercooled liquids. However, the parameter β_{KWW} can only reflects the degree of dynamical heterogeneity but cannot quantitatively describe nor determine the specific distribution of dynamic heterogeneity.

The heterogeneous microstructure of MGs is the origin of their unique mechanical properties. The structure of MGs is considered to be composed of different regions such as "solid-like region" and "liquid-like region" (Liu et al., 2011). The response of the solid-like region under external stress excitation is dominated by elasticity, and the response of the liquid-like region is inelastic. The free volume model proposed by Turnbull and Cohen (1970) explains that the total macroscopic volume of solids and liquids includes the actual occupied volume and free volume of atoms (or molecules). The free volume can be understood as voids around atoms which are randomly dispersed in the matrix with different sizes. Based on the work of Argon et al. (Argon, 1979; Argon and Shi, 1983), Falk and Langer (1998) proposed the shear transformation zone (STZ) model by taking specific atomic cluster in MGs under local shear stress as a basic unit of deformation. Perez (1990) defined the density fluctuations at nanoscale, accompanying with the fluctuations of entropy or enthalpy, as the quasi-point defect (QPD) to describe the evolution of dynamic relaxation and deformation behavior of MGs. The flow units model proposed by Wang and Wang (2018) regards the structure of MGs as some flow units embedded in an elastic matrix. Compared with the elastic matrix, the flow units have lower elastic modulus and hardness, and have faster dynamic characteristics.

Macroscopic mechanical models are helpful to obtain the constitutive relations of MGs and predict the mechanical behaviors, but they hardly reveal the nature of deformation as physical models. MGs should exhibit linear viscoelastic behavior under small oscillatory load, and their dynamic relaxation mainly occurs in the form of α relaxation and β relaxation. As a general characteristic of MGs, α relaxation provides an important way to understand the physical origin of the mechanical properties and important physical phenomena such as glass transition. Traditional mechanical models such as GKV and GM models can well describe the α relaxation spectrum of different MGs when there are enough elastic and viscous elements. Ju et al. (Ju and Atzmon, 2014; Ju et al., 2011) linked the discrete spectrum based on the GKV model with the STZs, and believed that the peaks on the discrete spectrum were related to STZs of different sizes. Traditional mechanical models usually require too many fitting parameters, and a promising solution relies heavily on the use of fractional calculus. Fractional calculus is a branch of mathematics, which extends integration and differentiation operators to non-integer order, to enrich the classical linear viscoelastic framework (Bonfanti et al., 2020). This led to a new development in modeling viscoelastic behaviors known as fractional viscoelasticity, which has been proved to be a good application in polymers (Metzler et al., 1995; Pritz, 2003; Wang and Kari, 2020).

Linear viscoelastic models are often presented as spectral models (Palade et al., 1996). Although direct measurement of the relaxation time spectrum is impossible, the main advantage of this modeling is to ensure consistency with linear viscoelastic theory and to easily solve the problem of converting dynamic data from frequency domain to time domain. Traditional mechanical models are able to combine the viscosity and elastic modulus with relaxation time, but still lack a specific physical interpretation. With the help of fractional calculus method, fractional viscoelasticity can express a specific distribution of relaxation time. At present, the application of fractional order model in polymers has a clear physical interpretation (Arikoglu, 2014; Sharma and Cherayil, 2010). It inspires further exploration in MGs using fractional order model which is necessary and of great importance.

As a typical CuZr-based MG, $Cu_{46}Zr_{47}Al_7$ MG is widely preferred for its good glass forming ability as well as suitable cost, in addition to its general properties of MGs (Jiang et al., 2006). At the same time, $Cu_{46}Zr_{47}Al_7$ MG can be used as a basic MG to consider the changes of various properties after micro-addition of other components (Xie et al., 2010; Xu et al., 2004). Thus, in the current work, the fractional order model was applied to $Cu_{46}Zr_{47}Al_7$ MG, which can be considered as a typical representative of MGs. Compared with the commonly used KWW function, the fractional order model is different in the description of the experimental phenomena and the

distribution of intrinsic relaxation times. To enrich the intrinsic origin of fractional viscoelasticity, we performed mathematical calculation to combine the fractional order model with the QPD theory, which has been widely used to describe the dynamic relaxations in MGs. Previous studies have observed the existence of "soft" regions in MGs, which are closely related to the deformation and reflect the structural heterogeneity (Wang et al., 2011; Yu et al., 2012). In order to verify this result, we discretized the relaxation times derived from the experimental data, and then combined the discrete spectral peaks with STZs according to Ju's viewpoint (Ju et al., 2011). The viscoelastic behaviors and relaxation spectrum of $Cu_{46}Zr_{47}Al_7$ MG were studied by the above methods to unveil the intrinsic heterogeneity in MGs.

2. Experimental procedures

2.1. Sample preparation

The model alloy with nominal composition $Cu_{46}Zr_{47}Al_7$ (at.%) (Xu et al., 2004) was prepared by arc-melting technique under purified argon atmosphere. In order to ensure compositional homogeneity, the ingots were melted at least six times. The ingot was then sucked into water-cooled copper mold to obtain the amorphous samples, with a size of 80 mm × 10 mm × 2 mm.

2.2. Materials characterization and thermal properties

The amorphous nature of the model alloy was determined by the X-ray diffraction (XRD). By Cu-Kα radiation, D8, Bruker AXS Gmbh was used and the scanning rate is 0.025° per step. As illustrated in the inset of Fig. 1(a), the broad diffraction peak can be seen clearly in the XRD pattern, which indicates the sample is in fully amorphous state.

The thermal properties of $Cu_{46}Zr_{47}Al_7$ MG were measured by a differential scanning calorimetry (DSC, Netzsch 404) at a heating rate of 10 K/min. According to the DSC curve in Fig. 1(a), the glass transition temperature T_g and the onset crystallization temperature T_x are respectively determined at 683 K and 756 K.

2.3. Dynamic mechanical analysis

The dynamic mechanical analysis of $Cu_{46}Zr_{47}Al_7$ MG was carried out on a homemade mechanical spectrometer within a high vacuum environment under an inverted torsion mode (as shown in Fig. 1(b)). The testing specimens have the approximate dimensions of 30 mm × 3 mm × 1 mm, and the surfaces of the specimens have been polished. The frequency-scan experiment was performed at fixed temperature by applying sinusoidal stress of various frequencies between 0.01 to 2 Hz. The amplitude of sinusoidal stress is very small, which will not lead to viscoplastic deformation. When sinusoidal stress is applied to viscoelastic materials, the strain has the same frequency, but there is a phase difference δ between the stress and strain. For an ideal elastic material, the phase difference is 0, while for a purely viscous material, the phase difference is $\pi/2$. The phase difference lies between 0 and $\pi/2$ for viscoelastic materials. The so-called complex modulus G^*, defined as $G' + iG''$, can be obtained from the experimental results. G' is the storage modulus and G'' is the loss modulus. In addition, the loss factor $\tan\delta$ can be defined by G''/G', where $\tan\delta$ is related to the energy loss of each cycle.

2.4. Nanoindentation experiments

In order to intuitively reflect the microstructural heterogeneity, nanoindentation experiments were carried out on Hysitron TI980 Triboindenter using Berkovich indenter at room temperature. Prior to the nanoindentation experiments, the sample was progressively polished to a mirror finish with sandpaper and diamond plaster to ensure accuracy during the experiments. To perform the mapping of local reduced modulus and hardness, an indentation matrix of 10 × 10 with 100 indents was conducted on the sample and the separation between indents was set as 30 μm to prevent the possible interaction of neighboring strain fields. Each indent was produced by

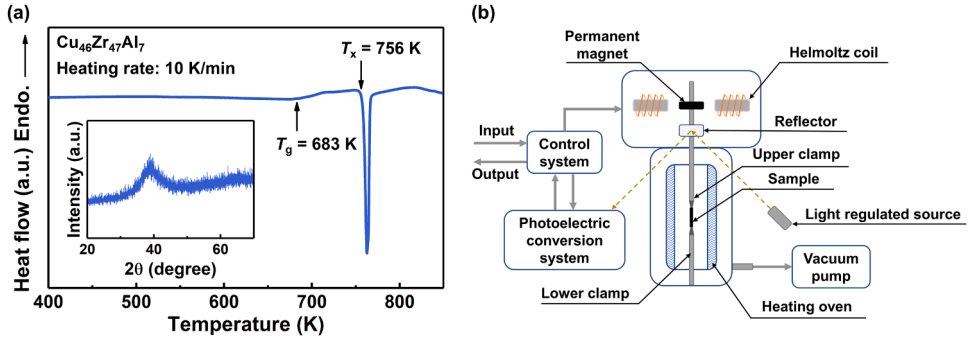

Fig. 1. (a) DSC curve of the $Cu_{46}Zr_{47}Al_7$ MG at a heating rate of 10 K/min. The inset exhibits the XRD pattern of the $Cu_{46}Zr_{47}Al_7$ MG. (b) Schematic diagram of the mechanical spectrometer.

applying a loading rate of 1 mN/s to 10 mN, and then unloading at the same rate immediately. The values of reduced modulus and hardness can be read directly from the results of Hysitron TI980 Triboindenter.

3. Theoretical model

The term "relaxation" is used to represent the process by which a system changes from a non-equilibrium state to an equilibrium state. In general, a relaxation process can be described by the function (Lukichev, 2019)

$$r(t) = r_\infty + r_0\phi(t) \tag{1}$$

where the r is a physical parameter of interest, r_0 and r_∞ are the constants, $\phi(t)$ is the normalized relaxation function.

Viscoelasticity is a typical mechanical characteristic of amorphous solids, and it is essentially a relaxation phenomenon. Viscoelastic behaviors are evident in experiments such as creep, stress relaxation and dynamic mechanical loading. Under the framework of linear viscoelasticity theory, the resultant stress function $\sigma(t)$ is linearly related to the increment step in strain magnitude of ε_0 at time $t = 0$

$$\sigma(t) = G(t)\varepsilon_0 \tag{2}$$

where $G(t)$ is the relaxation modulus, a monotonically decreasing function.

In Eq. (1), using σ instead of r, and then combining Eqs. (1) and (2), the relaxation modulus $G(t)$ can be expressed as

$$G(t) = \frac{\sigma_\infty}{\varepsilon_0} + \frac{\sigma_0}{\varepsilon_0}\phi(t) \tag{3}$$

where σ_0 and σ_∞ are constants. Similarly, for the stress step, creep compliance $J(t)$ can also be expressed as function of $\phi(t)$.

3.1. Debye relaxation and Zener model

For Eq. (1), the best-known relaxation function is the simple exponential function. It is also known as Debye relaxation that was used to research the motion of atoms in solid originally (Debye, 1929). Correspondingly, the normalized exponential relaxation function is

$$\phi(t) = e^{-t/\tau},\ t \geq 0 \tag{4}$$

where τ is the characteristic relaxation time. This parameter determines the rate of decrease (increase) of the relaxation function.

For the strain step (stress relaxation), we can write $G(t)$ in the form of Debye-type

$$G(t) = \frac{\sigma_\infty}{\varepsilon_0} + \frac{\sigma_0}{\varepsilon_0}e^{-t/\tau} \tag{5}$$

Time and frequency are inextricably linked, and the Laplace transform as a mathematical tool can realize the interconversion of time and frequency domains. Eq. (5) is transformed by Laplace transform to get

$$G^* = \frac{\sigma_\infty}{\varepsilon_0} + \frac{\sigma_0}{\varepsilon_0}\cdot\frac{i\omega\tau}{1+i\omega\tau} \tag{6}$$

The real part and imaginary part of Eq. (6) respectively represent the storage modulus $G'(\omega)$ and the loss modulus $G''(\omega)$, so

$$G'(\omega) = \frac{\sigma_\infty}{\varepsilon_0} + \frac{\sigma_0}{\varepsilon_0}\left(1 - \frac{1}{1+\omega^2\tau^2}\right) \tag{7a}$$

$$G''(\omega) = \frac{\sigma_0}{\varepsilon_0}\cdot\frac{\omega\tau}{1+\omega^2\tau^2} \tag{7b}$$

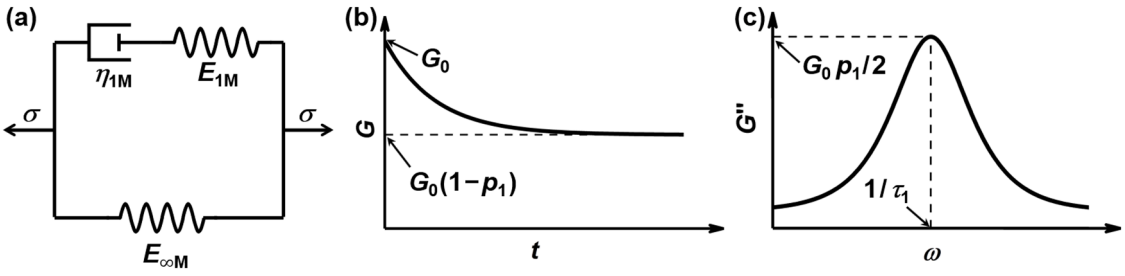

Fig. 2. (a) Skeleton of Zener model. (b) and (c) are the relaxation modulus and loss modulus of this model, respectively.

Many models and theories have been proposed to describe the viscoelastic behaviors, among which mechanical models consisting of spring (pure elastic) and dashpot (pure viscous) elements are well developed (Serra-Aguila et al., 2019). To gain some more intuitive comprehension of the viscoelastic behavior, it is useful to consider simple mechanical models with specific combinations of springs and dashpots. We firstly consider the well-known standard linear solid model (or Zener model), which can be interpreted by a combination of Hookean springs ($\sigma = E\varepsilon$) and a Newtonian dashpot ($\sigma = \eta \mathrm{d}\varepsilon/\mathrm{d}t$) with the spring constants E_{1M}, $E_{\infty M}$ and the viscosity η_{1M}, as shown in Fig. 2(a). After some simple calculations, the differential equation associated to the Zener model is

$$\sigma + \frac{\eta_{1M}}{E_{1M}} \cdot \frac{\mathrm{d}\sigma}{\mathrm{d}t} = E_{\infty M}\varepsilon + \frac{\eta_{1M}}{E_{1M}}(E_{\infty M} + E_{1M})\frac{\mathrm{d}\varepsilon}{\mathrm{d}t} \tag{8}$$

By applying a constant strain, the relaxation modulus can be given

$$G(t) = G_0\left[1 - p_1\left(1 - e^{-\frac{t}{\tau_1}}\right)\right] \tag{9a}$$

with

$$G_0 = E_{\infty M} + E_{1M}, \quad p_1 = \frac{E_{1M}}{E_{\infty M} + E_{1M}}, \quad \tau_1 = \frac{\eta_{1M}}{E_{1M}} \tag{9b}$$

The relaxation modulus of Zener model given in Eq. (9a) is the Debye form. In other words, Zener model and Debye relaxation are equivalent. Fig. 2(b) and (c) show the relaxation modulus and the loss modulus derived from Zener model, respectively. The Zener model has a single relaxation time, and it can be seen from the Fig. 2(c) that the loss modulus curve shows the form of symmetrical peak, which is different from the mechanical behavior of amorphous solids. According to the previous work, the loss modulus curve of amorphous solids shows an asymmetric curve (Bergman, 2000). Meanwhile, the relaxation function $\phi(t)$ of amorphous solids typically shows deviations from a single Debye relaxation, indicating that the relaxation time is actually not a single value. Continuous relaxation spectrum function with specific distribution $H(\tau)$ or discrete spectra with n pairs of relaxation strengths p_i and relaxation times τ_i can be considered. Then, the time relaxation function adopts the following forms respectively:

$$\phi(t) = \int_0^\infty H(\tau)e^{-t/\tau}\frac{\mathrm{d}\tau}{\tau} \tag{10a}$$

$$\phi(t) = \sum_{i=1}^{n} p_i e^{-t/\tau_i} \tag{10b}$$

3.2. Stretched exponential function

For the Eq. (1), amorphous solids often show deviations from the Debye form, and they are usually fitted with the stretched exponential function (or KWW function)

$$\phi(t) = e^{-\left(\frac{t}{\tau_{\mathrm{KWW}}}\right)^{\beta}}, \ 0 < \beta < 1 \tag{11}$$

where β is an empirical exponent. At present, there is no clear mathematical method to deal with the integral transformation of KWW function in spite of its simple form. As shown in Eq. (10a), relaxation functions featuring non-Debye form necessarily possess the spectrum of relaxation times. Therefore, the proper analysis and understanding of KWW function depend on its relaxation time spectra.

After some simple mathematical substitutions and the inverse Laplace transformations (Lindsey and Patterson, 1980), the relaxation time distribution $H(\tau)$ of KWW function can be obtained

$$H(\tau) = -\frac{\tau_{\mathrm{KWW}}}{\pi\tau}\sum_{k=0}^{\infty}\frac{(-1)^k}{k!}\sin(\pi\beta k)\Gamma(\beta k + 1)\left(\frac{\tau}{\tau_{\mathrm{KWW}}}\right)^{\beta k+1} \tag{12}$$

where Γ is the gamma function. Eq. (12) is the non-closed form, excluding $\beta = 1/2$. When $\beta = 1/2$, the distribution can be written in a closed form

$$H(\tau) = \frac{1}{2}\left(\frac{\pi\tau_{\mathrm{KWW}}}{\tau}\right)^{-\frac{1}{2}} e^{-\frac{\tau}{4\tau_{\mathrm{KWW}}}} \tag{13}$$

Due to the lack of mathematical method to perform Laplace transformation on Eq. (11), it is difficult to obtain the accurate expression in frequency domain. However, Bergman (2000) gives an approximate expression of the loss modulus in the frequency domain

$$\frac{G''}{G_u} = G_p'' \Big/ \left\{1 - \beta + \frac{\beta}{1+\beta}\left[\beta(\omega_p/\omega) + (\omega/\omega_p)^{\beta}\right]\right\} \tag{14}$$

where G_u is the storage modulus without relaxation, G_p'' is the peak value of the normalized loss modulus and ω_p is the loading frequency corresponding to the peak value.

For Eq. (14), in order to explore the change of loss modulus under different values of stretching parameter β, the values of G_p'' and ω_p are fixed as 0.25 and 1, respectively. Taking β as 0.2, 0.4, 0.5, 0.6 and 0.8, respectively, the normalized loss modulus curves corresponding to each β value are obtained, as shown in Fig. 3(a). It is found that the loss modulus curves are asymmetric in logarithmic frequency. The loss modulus at high frequency is significantly affected by the change of β. Meanwhile, it is found that the loss modulus peak gradually changes to the symmetric form with the increase of β. According to the Eq. (11), when β is equal to 1, the loss modulus shows the symmetric peak of the Debye form. In order to further analyze the distribution of internal relaxation times of loss modulus, we take $\tau_{\mathrm{KWW}} = 1/\omega_p$ and the distribution $H(\tau)$ corresponding to different values of β can be obtained, as shown in Fig. 3(b). $H(\tau)$ in Fig. 3(b) shows a strong dependence on the stretched parameter β. For the same β, as the relaxation time increases, the function shows the similar trend of initially increasing, reaching a maximum and then decreasing. Moreover, a narrow distribution is found for a larger value of β. The distribution of relaxation time can be seen as a reflection of the overall disorder of the system at the macroscopic level. The wider the distribution is, the more disordered the system is. On the contrary, a narrower distribution represents a more orderly system. When the distribution is concentrated to a single point in time, the system shows a Debye relaxation. Therefore, with the increase of parameter β, the disorder degree of the system decreases.

KWW function has been proved to be a good description for the viscoelastic behaviors of amorphous solids in previous work. It is worth mentioning that even if KWW function is suitable for describing various relaxation processes, its applicability should be considered when using this empirical function without theoretical proof (Apitz and Johansen, 2005). When there is more than one peak in the frequency domain, the parameters obtained from the use of a single KWW function may be unrealistic or even wrong. In this case, the superposition of multiple KWW functions will be relied on to correctly describe the relaxation process. Unfortunately, as an empirical equation, KWW function lacks physical interpretation.

3.3. Power law and fractional order model

For Eq. (1), in addition to the stretched exponential function (Eq. (11)), the asymptotic power-law is often used to describe relaxation deviating from Debye-form

$$\phi(t) = \frac{1}{(1+t/\tau)^{\alpha}} \sim \left(\frac{t}{\tau}\right)^{-\alpha} \tag{15}$$

where α is the power exponent. For the convenience of calculation and processing, the asymptotic power-law is often approximated by its corresponding long-time inverse power-law form, as shown in Eq. (15). Usually, Eq. (15) or the corresponding power law are referred to as Nutting law (Nutting, 1921). It should be noted that within a limited range of data, it is simply impossible to distinguish Eq. (11) or Eq. (15) by fitting.

One of the typical features of the non-Debye model of material relaxation is memory effect, i.e., the temporal correlation due to the fact that the current response is the sum of the incremental relaxation responses accumulated over a period of time (Schiessel et al., 1995). This property has been illustrated by Boltzmann in the superposition integral

$$\sigma(t) = \int_0^t G(t-\tau)\frac{\mathrm{d}\varepsilon(\tau)}{\mathrm{d}\tau}\mathrm{d}\tau \tag{16}$$

In order to describe the relaxation of power-law form, the relaxation modulus takes the form

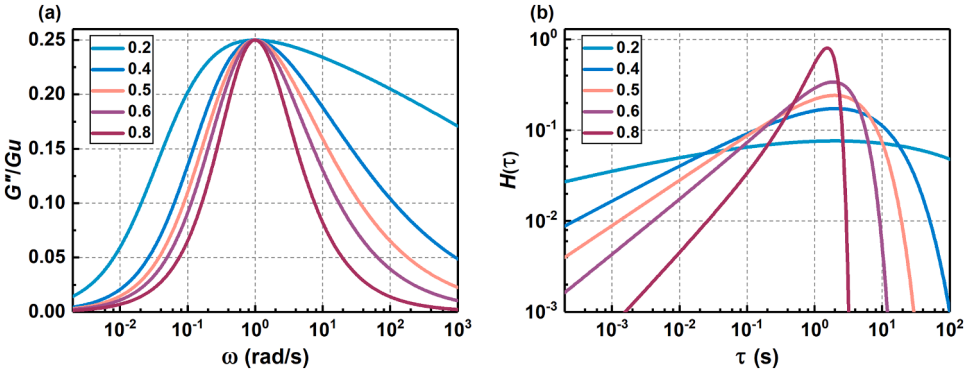

Fig. 3. (a) Normalized loss modulus curves calculated from the Eq. (14), where $G_p'' = 0.25$, $\omega_p = 1$ and the values of stretching parameter β is between 0.2 and 0.8. (b) Intensity of relaxation time $H(\tau)$ under different values of β.

$$G(t) = \frac{\sigma_\infty}{\varepsilon_0} + \frac{\sigma_0}{\varepsilon_0}\left(\frac{t}{\tau}\right)^{-\alpha} \tag{17}$$

Substituting this into Eq. (16), the relationship between stress and strain for a power-law material becomes:

$$\sigma(t) = \frac{\sigma_\infty}{\varepsilon_0}\varepsilon(t) + \frac{\sigma_0}{\varepsilon_0}\tau^\alpha \int_0^t (t-\tau)^{-\alpha}\frac{\mathrm{d}\varepsilon(\tau)}{\mathrm{d}\tau}\mathrm{d}\tau \tag{18}$$

Fractional calculus defines the differential operation of non-integer order or a function $f(t) = 0$ for $t < 0$ as (Gorenflo and Mainardi, 1997)

$$\frac{\mathrm{d}^\alpha f(t)}{\mathrm{d}t^\alpha} = \frac{1}{\Gamma(1-\alpha)}\int_0^t (t-\tau)^{-\alpha}\frac{\mathrm{d}f(\tau)}{\mathrm{d}\tau}\mathrm{d}\tau \tag{19}$$

Redefining the coefficient $c_\alpha = \tau^\alpha \Gamma(1-\alpha)\ \sigma_0/\varepsilon_0$ yields the following result:

$$\sigma(t) = \frac{\sigma_\infty}{\varepsilon_0}\varepsilon(t) + c_\alpha \frac{\mathrm{d}^\alpha \varepsilon(t)}{\mathrm{d}t^\alpha} \tag{20}$$

which provides a simple constitutive equation for the power-law materials. Fractional derivatives are nonlocal operators, which can effectively describe the memory effect and heredity properties of viscoelastic materials (Failla and Zingales, 2020).

Similar to KWW function, the fractional order model is capable of describing the linearly viscoelastic behavior with few parameters. For Eq. (20), σ_∞ is zero for convenience, and it can be described by a springpot element ($\sigma(t) = c_\alpha d^\alpha \varepsilon(t)/dt^\alpha$). The schematic symbol of springpot element and its relationship with the spring and dashpot elements are shown in Fig. 4. The springpot element, also known as the Scott–Blair's element (Blair and Veinoglou, 1944), can be understood as an interpolation element between the spring element ($\alpha = 0$) and the dashpot element ($\alpha = 1$). In order to test the application of fractional operators in viscoelastic materials, Bagley and Torvik (1983) have proved that the approach is consistent with molecular theories. At the same time, it is also confirmed that the fractional viscoelastic models have good consistency in thermodynamics (Friedrich, 1991; Gloeckle and Nonnenmacher, 1991).

Caputo and Mainardi (1971) first proposed the fractional Zener model by replacing integer derivative with fractional derivative in governing equation, which is a generalization of the Zener model, as shown in Fig. 5(a). The fractional Zener model has the specific relaxation time distribution, which can be used to describe the memory mechanism of materials. However, this model exhibits a Cole–Cole behavior, which is obviously inconsistent with the characteristics of amorphous solids.

In order to better predict the asymmetric loss modulus peak of amorphous solids and describe their mechanical behavior, the modified fractional (MF) model is adopted here (see Fig. 5(b)), which has been introduced by Heymans to overcome the problem of symmetrical loss peak (Heymans, 1996). The MF model, also as a generalization of the Zener model, is proposed by replacing the spring and dashpot in the Maxwell element with springpot elements, and attaching a spring to ensure that the high-frequency modulus is not infinite.

Considering that α_1 is greater than α_2, then according to the relationship between the elements, the governing equation of the MF model can be obtained

$$(E_1+E_2)\left(\sigma + \frac{c_{\alpha_1}}{c_{\alpha_2}}\cdot\frac{\mathrm{d}^{\alpha_1-\alpha_2}\sigma}{\mathrm{d}t^{\alpha_1-\alpha_2}}\right) + c_{\alpha_1}\frac{\mathrm{d}^{\alpha_1}\sigma}{\mathrm{d}t^{\alpha_1}} = E_1E_2\left(\varepsilon + \frac{c_{\alpha_1}}{c_{\alpha_2}}\cdot\frac{\mathrm{d}^{\alpha_1-\alpha_2}\varepsilon}{\mathrm{d}t^{\alpha_1-\alpha_2}}\right) + E_2 c_{\alpha_1}\frac{\mathrm{d}^{\alpha_1}\varepsilon}{\mathrm{d}t^{\alpha_1}} \tag{21}$$

In order to obtain the complex modulus of the MF model, the composition rule and Fourier integration for fractional calculus need to be applied (Schiessel et al., 1995). After some calculations and simplifications, we get

$$G^* = G_0 + (G_\infty - G_0)\frac{1}{1+\lambda(i\omega\tau_{\mathrm{MF}})^{-\alpha_2} + (i\omega\tau_{\mathrm{MF}})^{-\alpha_1}} \tag{22a}$$

where

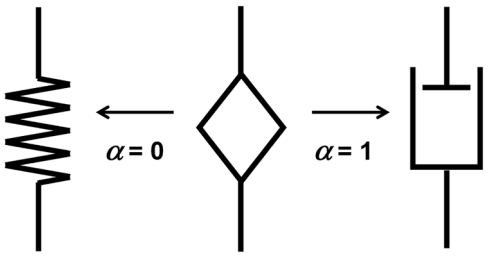

Fig. 4. Schematic diagram of the spring-pot element, which behaves as a spring when $\alpha = 0$ and as a dashpot when $\alpha = 1$.

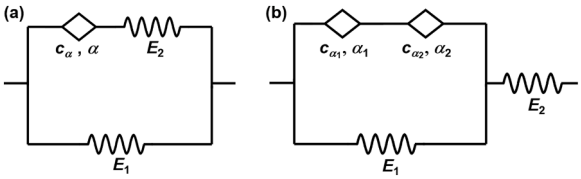

Fig. 5. (a) The fractional Zener model and (b) the modified fractional model.

$$G_0 = \frac{E_1 E_2}{E_1 + E_2},\ G_\infty = E_2,\ \tau_{\mathrm{MF}} = \left(\frac{c_{\alpha_1}}{E_1 + E_2}\right)^{\frac{1}{\alpha_1}},\ \lambda = \frac{c_{\alpha_1}}{c_{\alpha_2}}\left(\frac{E_1 + E_2}{c_{\alpha_1}}\right)^{\frac{\alpha_1 - \alpha_2}{\alpha_1}} \tag{22b}$$

The parameters G_0 and G_∞ correspond to the static modulus and the high-frequency modulus, respectively. τ_{MF} is the characteristic relaxation time of this model, and λ is the numerical factor. Then, we can get the loss modulus expression of the modified fractional model

$$G''(\omega) = \frac{(G_\infty - G_0)(\omega\tau_{\mathrm{MF}})^{\alpha_1}\left[\sin\left(\frac{\alpha_1\pi}{2}\right) + \lambda\sin\left(\frac{\alpha_2\pi}{2}\right)(\omega\tau_{\mathrm{MF}})^{\alpha_1 - \alpha_2}\right]}{1 + A(\omega\tau_{\mathrm{MF}})^{\alpha_1 - \alpha_2} + B(\omega\tau_{\mathrm{MF}})^{2(\alpha_1 - \alpha_2)}} \tag{23a}$$

where

$$A = 2\lambda\cos\left[\frac{(\alpha_1 - \alpha_2)\pi}{2}\right] + 2\cos\left(\frac{\alpha_1\pi}{2}\right)(\omega\tau_{\mathrm{MF}})^{\alpha_2} \tag{23b}$$

$$B = \lambda^2 + 2\lambda\cos\left(\frac{\alpha_2\pi}{2}\right)(\omega\tau_{\mathrm{MF}})^{\alpha_2} + (\omega\tau_{\mathrm{MF}})^{2\alpha_2} \tag{23c}$$

In order to obtain the relaxation time distribution $H(\tau)$ of the modified fractional model, we can take $\nu = 1/\tau_{\mathrm{MF}}$, where ν is the relaxation frequency. The spectrum is related to the normalized relaxation function $\phi(t)$ via

$$\phi(t) = \int_0^\infty h(\nu)e^{-\nu t}\mathrm{d}\nu \tag{24}$$

Laplace transform is taken on both sides of Eq. (24)

$$\frac{\phi^*(i\omega)}{i\omega} = \int_0^\infty \frac{h(\nu)}{\nu + i\omega}\mathrm{d}\nu \tag{25a}$$

with

$$\phi^*(i\omega) = \frac{1}{1 + \lambda(i\omega\tau)^{-\alpha_2} + (i\omega\tau)^{-\alpha_1}} \tag{25b}$$

Since the function $\phi^*(i\omega)/i\omega$ is the Stieltjes transformation of the relaxation spectrum $h(\nu)$, the relaxation spectrum $h(\nu)$ can be calculated by using the properties of the inverse Stieljes transformation (Tschoegl, 1989)

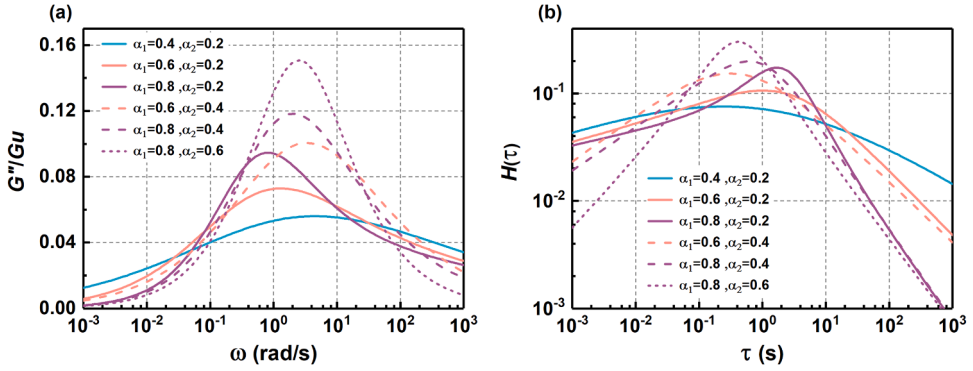

Fig. 6. (a) Normalized loss modulus curves calculated from Eq. (23a), where the values of parameter α_1 and α_2 are between 0.2 and 0.8. (b) Corresponding distribution of relaxation time $H(\tau)$ under different values of α_1 and α_2.

$$h(\nu)=\frac{1}{2\pi i}\left(\frac{\phi^*(\nu e^{-i\pi})}{\nu e^{-i\pi}}-\frac{\phi^*(\nu e^{+i\pi})}{\nu e^{+i\pi}}\right) \tag{26}$$

Combining Eqs. (10a) and (24), and taking the relaxation function (Eq. (25b)) into account at the same time, the relaxation time distribution $H(\tau)$ of the modified fractional model can be obtained

$$H(\tau)=\frac{1}{\pi}\cdot\frac{\left(\frac{\tau_{MF}}{\tau}\right)^{\alpha_1}\left[\sin(\alpha_1\pi)+\lambda\sin(\alpha_2\pi)\left(\frac{\tau_{MF}}{\tau}\right)^{\alpha_1-\alpha_2}\right]}{1+C\left(\frac{\tau_{MF}}{\tau}\right)^{\alpha_1-\alpha_2}+D\left(\frac{\tau_{MF}}{\tau}\right)^{2(\alpha_1-\alpha_2)}} \tag{27a}$$

where

$$C=2\lambda\cos[(\alpha_1-\alpha_2)\pi]+2\cos(\alpha_1\pi)\left(\frac{\tau_{MF}}{\tau}\right)^{\alpha_2} \tag{27b}$$

$$D=\lambda^2+2\lambda\cos(\alpha_2\pi)\left(\frac{\tau_{MF}}{\tau}\right)^{\alpha_2}+\left(\frac{\tau_{MF}}{\tau}\right)^{2\alpha_2} \tag{27c}$$

Although the parameters of the relaxation time distribution can be obtained by fitting specific loss modulus curve, it is more meaningful to explore the changes of this function relative to the τ_{MF}, λ, α_1 and α_2 parameters.

Fig. 6(a) shows the normalized loss modulus of the MF model as a function of frequency (Eq. (23a)), whereas the values of $(G_\infty - G_0)/G_\infty$, τ_{MF} and λ are fixed as 0.5, 1 and 1, respectively. It can be seen from the figure that different combinations of α_1 and α_2 leads to different frequency dependence of the loss modulus. Meanwhile, it can be found that $(G_\infty - G_0)/G_\infty$ and τ_{MF} do not strictly limit the peak value and peak frequency. Then, their relaxation time distribution $H(\tau)$ is given, as shown in Fig. 6(b). In general, with the increase of α_1 and α_2, the strength of loss modulus increases, and the change of relaxation time distribution is relatively complex, requiring more detailed comparison.

To further investigate the changes in the relaxation time distribution due to the changes of individual parameters, here we fix α_1 to be 1. The changes of relaxation time distribution relative to α_2 and λ are shown in Fig. 7(a) and 7(b), respectively. In Fig. 7(a), the maximum value of $H(\tau)$ gradually decreases as α_2 increases to ~0.4, and then develops a larger maximum value as α_2 is increased further. Similarly, we can see in Fig. 7(b) the influence of the λ parameter variation on the relaxation time distribution. In this case, the maximum value of $H(\tau)$ decreases and shifts to the left as the λ parameter increases. At the same time, the λ parameter increases, $H(\tau)$ becomes wider, which means that the relaxation time is distributed over a wider time range and the system becomes more disordered. However, according to Eq. (22b), there is a coupling relationship between the different parameters. It seems that it is difficult to match the real situation by simply changing a single parameter, although the numerical change of Eq. (27a) can be given. For all that, the MF model is advantageous in describing the non-Debye relaxation behaviors of amorphous solids, because it not only automatically satisfies the thermodynamic constraints, but also incorporates the memory effect through the fractional order operators. At the same time, the rich evolution of the relaxation time distribution brought about by changing the parameters also presents an opportunity to search for the physical origin of the MF model. In the following article, we will further enrich the content of the MF model from a microscopic perspective.

It is worth mentioning here that the above models are only suitable for describing a single asymmetric peak on the relaxation spectrum. When there are other obvious peaks (β relaxation, γ relaxation) in the mechanical relaxation spectrum except for α relaxation, it is difficult to correctly describe the whole relaxation process using the KWW function or the MF model alone. This is a promising solution to consider the superposition of models describing different relaxation processes (Reyes-Melo et al., 2004).

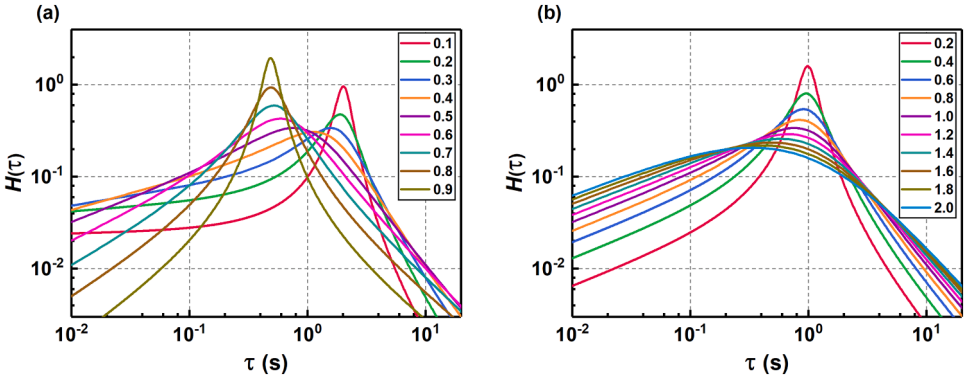

Fig. 7. Diagrams showing the change in the distribution of the relaxation time $H(\tau)$ for (a) $\alpha_2 = 0.1, 0.2, 0.3, \ldots, 0.9$ ($\tau_{MF} = 1$ s, $\lambda = 1$); (b) $\lambda = 0.2, 0.4, 0.6, \ldots, 2.0$ ($\tau_{MF} = 1$ s, $\alpha_2 = 0.5$).

3.4. Generalized Maxwell model

Two different forms of relaxation have been introduced aforementioned in viscoelastic materials. In such models, the distribution of relaxation times can be given based on the corresponding relaxation functions. Although the fitting of continuous relaxation time spectrum in experiments is satisfied, it remains to be discussed whether this is true for real distribution of relaxation times. Considering Eq. (10b), multiple discrete relaxation times are used to describe the real relaxation time distribution. Thus, the GM model is considered to further explore the intrinsic mechanism of viscoelastic behaviors.

A Maxwell element is composed of a spring and a dashpot in series. In order to describe the complex behaviors of viscoelastic materials, the schematic figure of GM model is presented in Fig. 8 which contains n maxwell elements and one spring element with all elements in parallel.

The strain ε in each Maxwell element should be same, equal to the sum of the strain of the spring $\varepsilon_i^{\mathrm{e}}$ and the dashpot $\varepsilon_i^{\mathrm{v}}$ in this Maxwell element. Therefore, we have

$$\varepsilon = \varepsilon_i^{\mathrm{e}} + \varepsilon_i^{\mathrm{v}},\ i = 1..n \tag{28}$$

Then, the total stress is given by

$$\sigma = E_{\infty M}\varepsilon + \sum_{i=1}^{n} E_{iM}\varepsilon_i^{\mathrm{e}} \tag{29}$$

Through a series of processing of the stress-strain relationship of the GM model, the relaxation modulus can be given

$$G(t) = G_0\left[1 - \sum_{i=1}^{n} p_i\left(1 - e^{-\frac{t}{\tau_i}}\right)\right] \tag{30a}$$

with

$$G_0 = E_{\infty M} + \sum_{i=1}^{n} E_{iM},\ p_i = \frac{E_{iM}}{E_{\infty M} + \sum_{i=1}^{n} E_{iM}},\ \tau_i = \frac{\eta_{iM}}{E_{iM}},\ i = 1..n \tag{30b}$$

The storage modulus and loss modulus of GM model are given as following

$$G'(\omega) = G_0\left[1 - \sum_{i=1}^{n} \frac{p_i}{1 + \tau_i^2\omega^2}\right] \tag{31a}$$

$$G''(\omega) = G_0 \sum_{i=1}^{n} \frac{p_i\tau_i\omega}{1 + \tau_i^2\omega^2} \tag{31b}$$

For the GM model, it can be seen that the relaxation spectrum is a discrete spectrum in the form of Eq. (10b), which cannot be given explicitly as in the two previous models. Although the GM model is not limited to the specified relaxation time distribution, the value of n should be large enough to obtain sufficiently accurate results, which will increase the computational effort significantly.

4. Result and discussion

4.1. DMA as a function of frequency

DMA is essentially a thermal and mechanical coupling process, which is convenient to measure the viscoelastic response under oscillating deformation (Hao et al., 2022). For MGs, the dynamic mechanical behavior depends on the driving frequency and

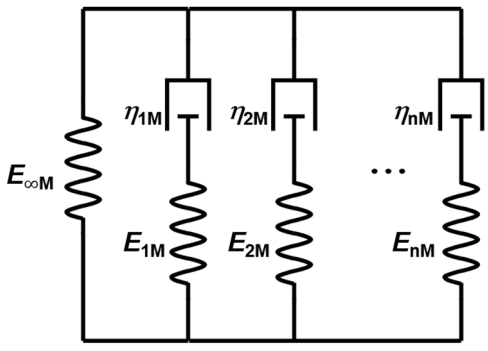

Fig. 8. Generalized Maxwell model.

temperature (Menard and Menard, 2020). Fig. 9(a) and (b) show the normalized storage modulus $G^{'}/G_u$ and loss modulus $G^{''}/G_u$ of $Cu_{46}Zr_{47}Al_7$ MG as a function of driving frequency with a temperature interval of 5 K, respectively. The decrease of storage modulus $G^{'}$ with the increase of temperature (or the decrease of frequency) indicates that the mechanical behavior of $Cu_{46}Zr_{47}Al_7$ MG changes from elasticity to viscoelasticity upon heating or slowing down of oscillation. At higher temperature, the peak of loss modulus becomes obvious due to the existence of α relaxation, which is the characteristic of amorphous materials (Pelletier et al., 2002). At the same time, the α relaxation peak gradually shifts to the lower frequency direction with the decrease of temperature. It should be noted that there is no obvious β relaxation behavior in the loss modulus, even if the temperature has been reduced below the glass transition temperature. This phenomenon is similar to that observed in other CuZr-based MGs, which usually show the form of excess wing (Qiao et al., 2019).

The lower frequency means longer time for atoms to migrate during one cycle of oscillation. The macroscopic flow thus become more pronounced. Correspondingly, higher temperature can improve the atomic mobility and thus increase the macroscopic flow. Specifically, the characteristics of the sample as temperature increases can also be shown when the frequency decreases, which is seen in Fig. 9. Therefore, the effects of frequency and temperature on the viscoelasticity are equivalent to some extent. This is the basic idea of time-temperature superposition (TTS) principle (Bergeret et al., 1992), which can be used to obtain the master curve of the normalized loss modulus in a broadened frequency domain.

By applying the TTS principle, the master curve can be obtained by horizontally shifting the curves of different temperatures into a reference temperature. The reference temperature is set as 700 K in the current work, and the master curve of the normalized loss modulus is shown in Fig. 10(a). It is necessary to take into account the validity when using the TTS principle, that is, only the relaxation curves with the shape independent of temperature can be taken. For $Cu_{46}Zr_{47}Al_7$ MG, it can be found that the shape of the master curve is similar to the curves at other temperatures, indicating that temperature has little effect on the relaxation breadth, and the contribution of β relaxation can also be ignored. In addition, the shifted data points are averaged to optimize the master curve, as shown in Fig. 10(b).

Previous work has shown that the α relaxation peak in the frequency spectrum can be well described by the KWW function (Eq. (14)) (Qiao and Pelletier, 2014b). The value of β can be obtained from the fitting of KWW equation, as the solid line shown in Fig. 10 (b). β is determined to be ~0.53. The value of β is similar to those obtained in other CuZr-based MGs (Qiao et al., 2016; Tao et al., 2021). At the same time, the value of characteristic relaxation time τ_{KWW} based on the form of extended exponential equation is ~29.7 s. It should be noted that in the high-frequency tail of the master curve, there is a small deviation between the data points and the KWW fitting curve, which may be caused by the β relaxation in the form of excess wing. Although the KWW function can well describe the α relaxation, its physical meaning is still not very clear. Wang et al. (2014) linked β with the degree of dynamic heterogeneity in the supercooled liquid, and a smaller β usually represents a larger dynamic heterogeneity of the system. Lukichev (2019), based on the mechanical oscillator model, argued that the KWW function describes the motion related to coordinate dependent viscosity.

Fractional rheology based on the power law has been proved to be satisfactory description of the viscoelastic behavior in polymers (Fang et al., 2015; Nadzharyan et al., 2018). In our work, the MF model is proposed to be combined with Zener model and the fractional element, which is used to describe the dynamic response of MGs. At the same time, we take α_1 as 1, which will be introduced later. The fitting result of MF model (Eq. (23a)) is shown in the dotted line in Fig. 10(b). It can be found that the MF model is in good agreement with the data points in the whole observation frequency range. Compared with the KWW function, MF model can describe the viscoelastic behavior of $Cu_{46}Zr_{47}Al_7$ MG in a wider frequency range. It implies that the fractional rheological model can be also used in MGs.

4.2. Physical origin of the MF model

In polymers, the fractional rheological model has been explained by the generalized Langevin equation (Sharma and Cherayil, 2010). In order to explore the physical interpretation of MF model, τ_{mol} and χ are used instead of τ_{MF} and α_2, respectively. For MGs, the

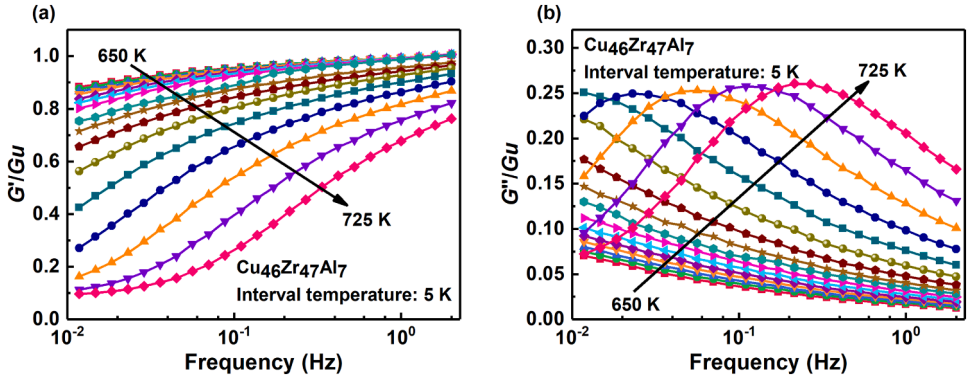

Fig. 9. DMA curves in the $Cu_{46}Zr_{47}Al_7$ MG as a function of frequency at various temperatures (650 to 725 K by step of 5 K). (a) The normalized storage modulus $G^{'}/G_u$ and (b) the normalized loss modulus $G^{''}/G_u$, respectively.

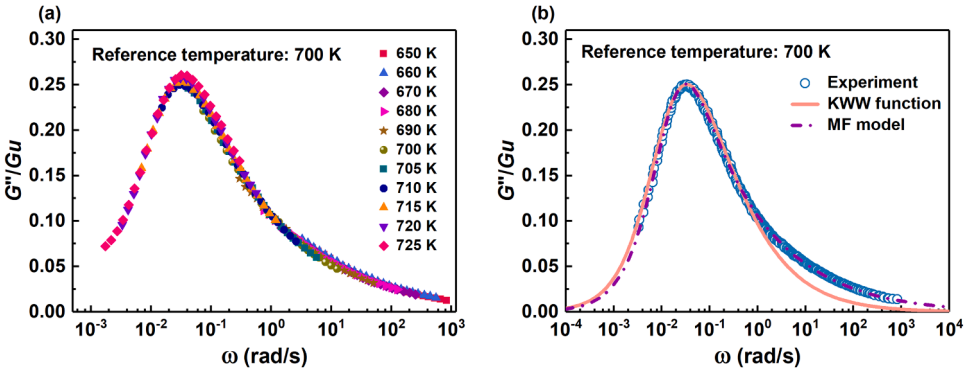

Fig. 10. (a) Master curve obtained by TTS principle. (b) Description of the experimental data by different models. The solid line is fitted by the KWW equation, where $\beta = 0.53$ and $\tau_{KWW} = 29.7$ s. The dotted line is fitted by the MF model, where $(G_\infty - G_0)/G_\infty = 0.94$, $\tau_{MF} = 35.1$ s, $\lambda = 0.99$ and $\alpha_2 = 0.35$.

α_1 parameter can be considered equal to 1 (Cavaillé et al., 1991; Pelletier et al., 2002; Qiao and Pelletier, 2014a). Thus, Eq. (22a) can be rewritten as

$$G^* = G_0 + (G_\infty - G_0)\frac{1}{1 + \lambda(i\omega\tau_{\mathrm{mol}})^{-\chi} + (i\omega\tau_{\mathrm{mol}})^{-1}} \tag{32}$$

where χ is a correlation factor. Eq. (32) is the frequency domain expression of the QPD theory. Perez et al. (Perez, 1990; Perez et al., 1983) proposed the QPD theory based on the concept of "quasi-point defects", which was first used to describe the relaxation mechanism and the mechanical deformation mechanism of amorphous polymers. In the framework of QPD theory, density fluctuations accompanied by fluctuations in entropy or enthalpy in amorphous materials are considered as quasi-point defects. In the process of nucleation, merging and expanding of the quasi-point defects, atoms or molecules of glass forming liquid can move relatively, resulting in a macroscopic dynamic relaxation behavior. According to QPD theory, the global characteristic relaxation time τ_{mol} of atoms or molecules in amorphous materials can be defined as (Mangion et al., 1992; Pelletier et al., 2002):

$$\tau_{\mathrm{mol}} = t_0\left(\frac{\tau_\beta}{t_0}\right)^{1/\chi} \tag{33}$$

where t_0 is a time scale factor. τ_β is the characteristic time of the elementary movements related to β relaxation, which follows the Arrhenius law:

$$\tau_\beta = \tau_{0\beta}\exp\left(\frac{U_\beta}{kT}\right) \tag{34}$$

where U_β is the activation energy of β relaxation, k is the Boltzmann constant, T is the absolute temperature, and $\tau_{0\beta}$ is a pre-exponential factor.

Due to the disordered arrangement of atoms in MGs, the activation energy U_β in Eq. (34) should adopt a distribution function instead of a single value (Egami, 2011; Yang et al., 2012). Previously, lognormal distribution or discretized normalized Gumbel distribution is often used to describe the distribution of τ_β (Hao et al., 2022; Rinaldi et al., 2011). In this work, we take a continuous function to describe the asymmetric distribution, as given in Eq. (12). Thus, $\langle\tau_\beta\rangle$ should be used instead of τ_β in Eq. (33), where $\langle\tau_\beta\rangle$ is the most probable value of τ_β. Rinaldi et al. (2011) argued that there are four contributions of deformation in QPD theory based on hierarchical correlation, including elastic component, β relaxation, and the viscoelastic and viscoplastic components of α relaxation. Here, the expression of complex compliance J^* is given

$$J^* = \frac{1}{E_{\mathrm{el}}} + A_\beta\int_0^\infty \frac{H(\tau_\beta)}{1 + i\omega\tau_\beta}\mathrm{d}\ln\tau_\beta + A_{\mathrm{ve}}\int_0^\infty \frac{H(\tau_{\mathrm{ve}})}{1 + i\omega\tau_{\mathrm{ve}}}\mathrm{d}\ln\tau_{\mathrm{ve}} + A_{\mathrm{vp}}\int_0^\infty \frac{H(\tau_{\mathrm{vp}})}{1 + i\omega\tau_{\mathrm{vp}}}\mathrm{d}\ln\tau_{\mathrm{vp}} \tag{35}$$

where E_{el} is storage modulus at ambient temperature. A_β, A_{ve} and A_{vp} are regarded as the intensity of the β relaxation process, viscoelastic deformation and viscoplastic deformation. Meanwhile, τ_β, τ_{ve} and τ_{vp} are considered as the relaxation time of the above three processes, respectively. Note that G^* in Eq. (32) is simply the inverse of the J^* expression. This means that both the storage modulus G' and the loss modulus G'' can be simply deduced from J' and J''.

Considering the range of temperature and frequency in which the DMA experiment were conducted, the viscoplastic deformation component in Eq. (35) can be neglected. Thus, the viscoelastic deformation component can be equivalent to contribution of α relaxation. In this case, Eq. (35) can be rewritten as

$$J^* = \frac{1}{E_{\mathrm{el}}} + A_\beta \int_0^\infty \frac{H(\tau_\beta)}{1 + i\omega\tau_\beta} \mathrm{d}\ln\tau_\beta + A_\alpha \int_0^\infty \frac{H(\tau_\alpha)}{1 + i\omega\tau_\alpha} \mathrm{d}\ln\tau_\alpha \tag{36}$$

where A_α and τ_α are the intensity and relaxation time of α relaxation, respectively. In addition, because of the asymmetry of α relaxation process, here τ_α adopts the same distribution as τ_β. At this point, the loss modulus can be understood as a superposition of two KWW functions with different empirical exponents ($\beta_{\mathrm{KWW}-\alpha}$, $\beta_{\mathrm{KWW}-\beta}$) and characteristic relaxation time ($\tau_{\mathrm{KWW}-\alpha}$, $\tau_{\mathrm{KWW}-\beta}$), as shown in Fig. 11(a). It can be seen that the calculated master curve is able to fit the experimental data better compared to the use of a single KWW function. Moreover, the β relaxation in the form of excess wing is successfully separated from the master curve. The contributions of different components to the relaxation time distribution are given in Fig. 11(b). Furthermore, it can be seen that the relaxation time distribution obtained from the superposition of two components deviates from the distribution given by the QPD theory, although they are very close in the description of the main curve. This implies that the QPD theory is not simply a superposition of two KWW functions, and as mentioned before there are essential differences between them. Nevertheless, due to the difficulty of deconstructing Eq. (27a) directly, giving a priori distributions of relaxation time for different processes is still very relevant for a deeper understanding of the QPD theory.

In QPD theory, the correlation factor χ, corresponding to α_2 in Eq. (22a), is closely related to the concentration of quasi-point defects, which reflects the degree of short-range order, and can quantitatively indicate the atomic mobility of amorphous materials and the change of quasi-point defects concentration in the relaxation process. When the value of χ is 0, the material is completely ordered, corresponding to the ideal crystal. The motion of atoms or molecules is completely related, and the motion of structural units is affected by the motion of all other units. At this time, the concentration of quasi-point defects in the system is the smallest. On the contrary, when the value of χ is 1, the material is completely disordered, corresponding to the ideal gas. The motion of all structural units is independent of each other and the quasi-point defect concentration reaches the maximum. The loss factor $\tan\delta$, defined as the ratio of loss modulus to storage modulus G''/G', is an important factor to reflect how much materials can lose energy due to dynamic deformation. In the framework of QPD theory, the evolution of loss factor $\tan\delta$ of amorphous materials with frequency can be expressed as

$$\ln(\tan\delta) = -\frac{U_\beta}{kT} - \chi\ln(\omega) - \chi\ln(\tau^*) + \ln(\lambda) \tag{37}$$

where τ^* corresponds to the mean time required for the structural unit to move over its equal size distance. Below T_g, MGs remain in an isoconfigurational state and thus the value of χ is constant, so the Arrhenius behavior can be expected. On the contrary, metastable thermodynamic equilibrium will occur when temperature is above T_g, and χ increases with temperature. In a first approximation, the evolution of correlation factor χ with temperature can be assumed to obey simple forms

$$\chi(T) = \chi(T_g) \text{ for } T < T_g, \tag{38a}$$

$$\chi(T) = \chi(T_g) + a(T - T_g) \text{ for } T \geq T_g \tag{38b}$$

where a is the slope.

Fig. 12(a) shows the logarithmic relationship between the loss factor $\tan\delta$ and angular frequency ω of $Cu_{46}Zr_{47}Al_7$ MG at different temperatures. The correlation factor χ can be determined by the slope of the solid line fitted by Eq. (37). It can be seen that the experimental data between 650~710 K can be well described by Eq. (37). Fig. 12(b) shows the evolution of correlation factor χ with temperature. It can be found that the evolution of correlation factor with temperature conforms to Eq. (38). As shown in Fig. 12(b), the

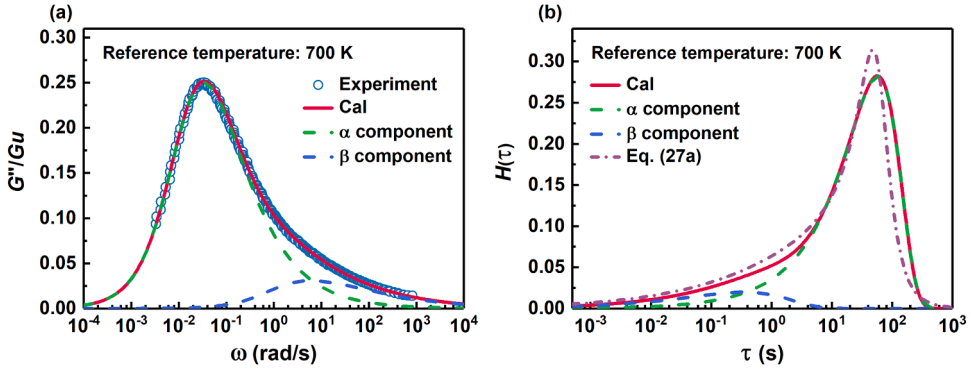

Fig. 11. (a) Master curve of the normalized loss modulus. Red solid line: calculated curve. The dashed lines respectively denote individual contributions to the α and β relaxations, where $\beta_{\mathrm{KWW}-\alpha} = 0.58$, $\tau_{\mathrm{KWW}-\alpha} = 29.7$ s, $\beta_{\mathrm{KWW}-\beta} = 0.41$, $\tau_{\mathrm{KWW}-\beta} = 0.17$ s, and $A_\alpha/A_\beta = 8.1$. (b) The dashed lines indicate the separate contributions of α and β relaxation to the relaxation time distribution, respectively. The red solid line is a superposition of the contributions from α component and β component. The dotted line is fitted by the MF model.

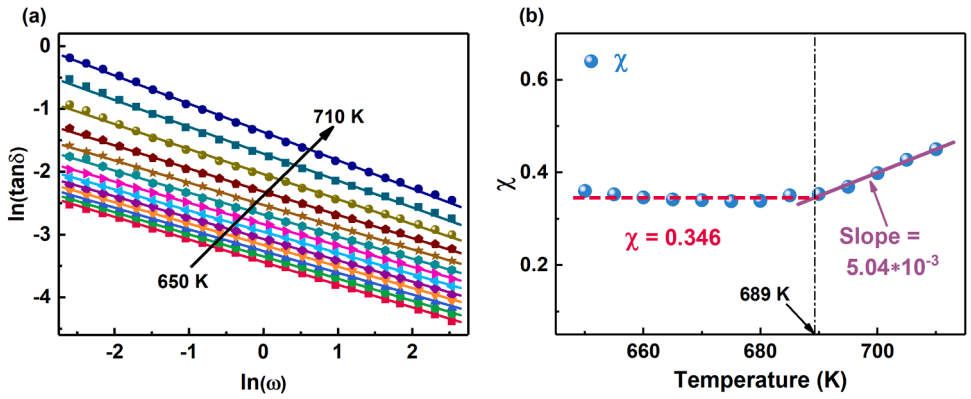

Fig. 12. (a) Influence of the driving frequency on the logarithm of the loss factor tanδ at different temperatures. The solid lines represent theoretical fits by Eq. (37); (b) Evolution of the correlation factor χ with temperature.

parameter χ remains around constant when the temperature below T_g due to the glassy solids stay in isoconfigurational state. The glass transition temperature can be determined around 689 K, which is very close to the 683 K obtained from the DSC curve. The values of χ below T_g are between 0.3 and 0.4 for most typical MGs (Zhang et al., 2021), the value of χ below T_g in the current work is determined to be 0.346, which is consistent with other works in the literature. According to the QPD theory, the structure in the amorphous system is in a frozen state below T_g, thus the concentration of quasi-point defects remains almost constant and the atomic mobility is limited. Above T_g, a large number of frozen atoms are activated and the concentration of quasi-point defects increases with the increase of temperature, resulting in a significant increase in χ. Fig. 12(b) shows a linear increase of the correlation factor χ above T_g and the slope is determined to be 5.04×10^{-3}.

In previous reports, the microstructure heterogeneity of MGs was qualitatively described based on concentration of defects, which was considered to be closely related to plastic deformation (Gao and Bei, 2016; Li et al., 2015; Qiao et al., 2019). KWW function was widely used in the research of MGs, and the parameter β can qualitatively describe the dynamical heterogeneity (Wang et al., 2014). Here we list the β of some MG systems to compare with the corresponding χ in QPD theory, as shown in Table 1. It can be seen that the MF model based on QPD theory can be well applied to various MGs. In particular, QPD theory can accurately describe the decrease of concentration of defects after annealing (Qiao et al., 2017). Meanwhile, in the process of microalloying, the elaboration of defect evolution in QPD theory is consistent with KWW function (Tao et al., 2021).

4.3. *Discretization analysis of the microstructure of MGs*

The explicit expressions of relaxation time distributions based on the KWW function and the power-law form can be given in continuous forms, however, the intrinsic nature of the discrete atoms in MGs indicates that the true distribution might be discrete rather than continuous. Recently, in the quasistatic measurements of the amorphous $Al_{86.8}Ni_{3.7}Y_{9.5}$ ribbon, Ju et al. (2011) successfully obtained the distribution of discrete relaxation times and revealed the quantized hierarchy of STZs with the help of direct spectrum analysis. Jiao et al. (2013) proposed that MGs may be composed of an elastic matrix and a series of scattered deformation units, and gave evidence for structural heterogeneity by analyzing deformation units with various relaxation times in the Pd-based MG. In nanoindentation pop-in tests, Gao and Bei (2016) employed the unified model to describe the defect density of MGs, and proposed a phenomenological model of ductile-versus-brittle behavior based on hard matrix and soft zones at the micro scale. Ke et al. (2014) and Tao et al. (2022) gave the direct reflection of the structural heterogeneity by conducting the local indentation matrix in nanoindentation experiments of MGs. In order to acquire the distribution of local mechanical properties of the $Cu_{46}Zr_{47}Al_7$ MG, the nanoindentation experiments were repeated at 10×10 different positions in a square lattice with a spacing of 270 μm. Fig. 13(a) and (b) show the mapping of local reduced modulus and local hardness as obtained from the nanoindentation experiments. As illustrated in this figure, the tested amorphous structure exhibits the variations in the local static property, which indicates the microstructural heterogeneity. Fig. 13(c) and (d) display the statistical distributions of local reduced modulus and local hardness, all of them can be

Table 1
Chemical composition, glass transition temperature T_g, empirical exponent β and correlation factor χ for some MGs.

Metallic glasses	T_g (K)	β	χ (below T_g)
$Cu_{46}Zr_{47}Al_7$ (current work)	683	0.53	0.346
$Cu_{46}Zr_{46}Al_8$ (as-cast) (Qiao et al., 2017)	691	–	0.37
$Cu_{46}Zr_{46}Al_8$ (annealed at 623 K) (Qiao et al., 2017)	–	–	0.34
$Zr_{50}Cu_{40}Al_{10}$ (Tao et al., 2021)	691	0.49	0.383
$(Zr_{50}Cu_{40}Al_{10})_{98}Dy_2$ (Tao et al., 2021)	683	0.48	0.395
$Pd_{43}Ni_{10}Cu_{27}P_{20}$ (Pelletier et al., 2002)	568	0.5	0.40
$(LaCe)_{32.5}Co_{20}Al_{15}$ (Zhai et al., 2018)	422	0.463	0.44

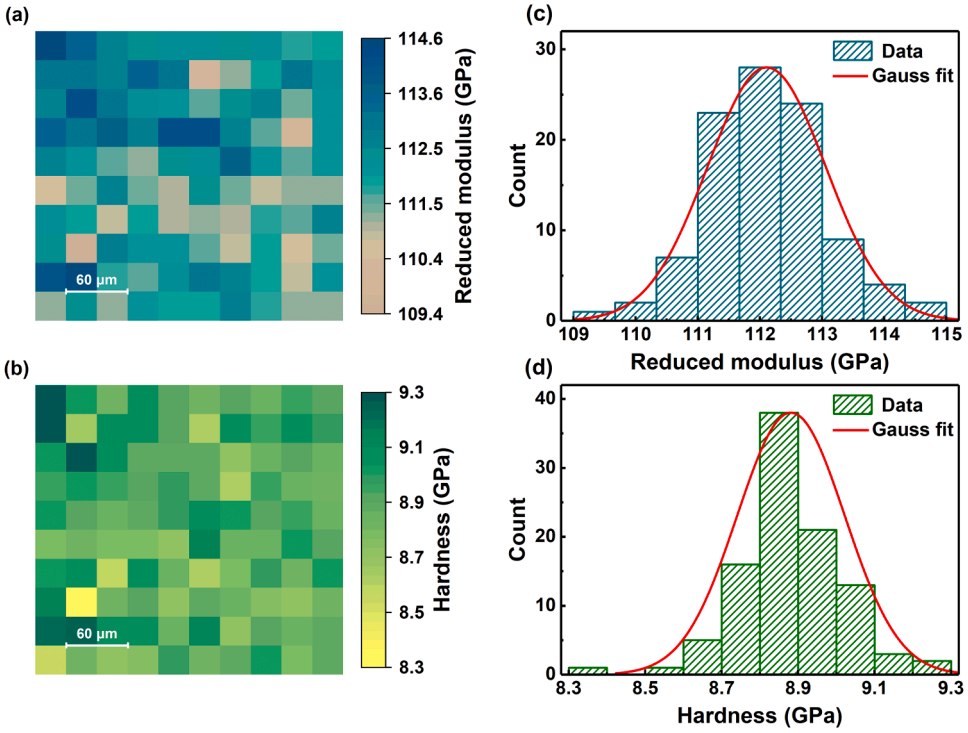

Fig. 13. Mapping of (a) local reduced modulus and (b) local hardness of $Cu_{46}Zr_{47}Al_7$ MG at the indentation load of 10 mN and the scanning space of 270 μm. On the right are the corresponding statistical distribution of (c) local reduced modulus and (d) local hardness. The red dashed lines are the Gaussian fitting to the experimental data.

well fitted to the Gaussian curve, which is consistent with the previous investigations (Ke et al., 2014; Tao et al., 2022; Wagner et al., 2011).

The dynamical heterogeneity seems to arise from the structural heterogeneity (Jiao et al., 2013), in the concept of dynamic heterogeneity, there are various local regions with different sizes in the MGs where atoms move at different rates, thus leading to different relaxation times in these regions (Berthier, 2011) (as is schematically displayed in the illustration in Fig. 14). These local relaxation behaviors contribute to the overall relaxation, and the discrete distribution of relaxation time can be obtained by collecting the characteristic relaxation times of different regions. For $Cu_{46}Zr_{47}Al_7$ MG, Fig. 14 shows the schematic diagram of contributions of different regions to the overall relaxation. Each region only has one single characteristic relaxation time, and its response is considered to conform to a Debye relaxation behavior (as shown in Eq. (4)). In order to further explore the real change of the intrinsic relaxation times, the GM model is used, and each region is equivalent to a Maxwell element (as illustrated in Fig. 8).

As described above for the GM model, Eq. (31b) can be used to fit the loss modulus as a function of frequency. The number of

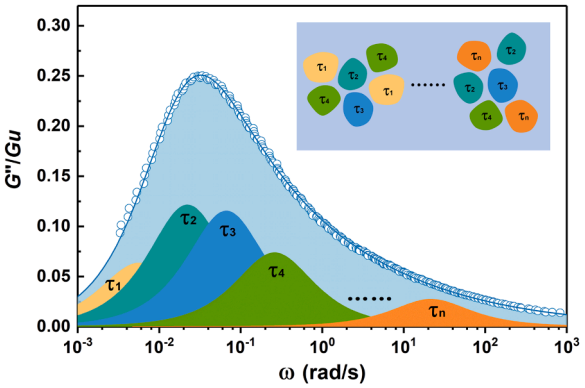

Fig. 14. Schematic diagram of the relaxation spectrum and the decomposed independent relaxation times. The solid line is the best fitting of the QPD model. The inset is a schematic illustration of the corresponding spatial distribution of the heterogeneous relaxation time domains in $Cu_{46}Zr_{47}Al_7$ MG.

Maxwell elements, n, should be as large as possible to ensure that the calculated relaxation time distribution is smooth enough. At the same time, a large value of n means that more computational resources are required. In addition, n should not exceed the number of data points to avoid the uncertainty of the solution. The p_i are fitting parameters, and the τ_i are fixed and spaced logarithmically. Owing to the reciprocal relationship between relaxation time and angular frequency, there are $\tau_{\min} = 1/\omega_{\max}$ and $\tau_{\max} = 1/\omega_{\min}$. In the current work, n is set as 80 and the corresponding relaxation times are set to be equally logarithmic spaced from $\tau_{\min} = 1/4\omega_{\max}$ to $\tau_{\max} = 4/\omega_{\min}$, so as to obtain the change of relaxation time in a relatively wide range. In order to make the calculation result converge better, $p_1 = 0$ and $p_{80} = 0$ are taken as boundary conditions. In the calculation process, the regularization factor is introduced to prevent over fitting. According to Eq. (10b), the intensity of the relaxation time spectrum, $H(\tau_i)$, is given by

$$H(\tau_i) = p_i/\Delta\ln\tau. \tag{39}$$

The calculation results are shown in the histogram in Fig. 15. To further compare with the continuous spectrum of relaxation time, the relaxation time distribution derived from KWW function and MF model are obtained according to Eq. (12) and (27a). For the model with continuous spectrum, the relaxation time distribution shows only a single peak. As shown in Fig. 15, the MF model shows a narrower and higher peak, while the distribution peak of KWW function is broader and lower. For the discrete relaxation time spectrum, although the overall trend is similar to the continuous spectrum, there are many small peaks, which reflects the dynamic heterogeneity in MGs.

The relationship between the relaxation time τ and the activation energy spectrum E_a is $\tau = \tau_0\exp(E_a/KT)$. Moreover, the activation energy spectrum in fact approximately conforms to the Gaussian distribution. In this context, Jiao et al. (2013) and Liu et al. (2022) speculate that the relaxation time spectrum conforms to the lognormal distribution, and the stress relaxation experimental data can be well described by the flow unit model. As shown in Fig. 16, by further processing the discrete relaxation time spectrum, it can be found that each peak can be well described by the log-normal distribution. According to the results, we infer that the relaxation time distribution in MGs should be the superposition of multiple log-normal distribution processes, rather than a simple log-normal distribution. This fact further reflects the heterogeneity of the internal structure of MGs. Lei et al. (2020) deemed that the peaks on different time scales correspond to different processes in MGs. The peaks near the relaxation time corresponding to the peak frequency of loss modulus show a wider and higher form, which correspond to the α relaxation process. At the same time, the small peaks at the smaller time scale are considered as evidence of the existence of the β relaxation.

The discretization of the peaks in relaxation time distribution directly reflects the differences of relaxation times between different regions. The difference of dynamic response originates from the microstructural heterogeneity in MGs. Ju et al. (Ju and Atzmon, 2014; Ju et al., 2011) associated discrete peaks of relaxation time distribution to STZs in MGs. In the presence of shear stress, small clusters composed of multiple atoms will spontaneously rearrange cooperatively (Argon, 1979). Clusters migrate across the energy barrier to a lower energy state, and inelastic shear deformation occurs in the system. In the process of continuous loading, the local plastic flow in the STZ causes more local STZs through percolation. These STZs expand and merge with each other, and finally show macro shear zones. The strain of MGs is mainly concentrated in the shear band with a thickness of only tens of nanometers (Qiao et al., 2019; Van Loock et al., 2021). Through the multi-peaks fitting of the discrete relaxation time spectrum, there are 11 distinct peaks in Fig. 16. Each peak can be considered to corresponds to a specific type of STZs (see the inset of Fig. 16). As mentioned by Ju et al. (2011), the area of a peak m represents the volume fraction occupied by potential m-type STZs, and there are atomic level differences between different types of STZs. Therefore, the discrete relaxation time distribution reveals the discrete nature of microstructure in MGs, which also helps us understand the diversity of STZs in MGs.

5. Conclusion

In this work, the dynamic mechanical spectrum of a $Cu_{46}Zr_{47}Al_7$ MG in frequency domain is probed by means of DMA technique. When describing the non-Debye relaxation, the MF model is proposed based on the fractional rheology in addition to the commonly used KWW function, and both models can well describe the experimental data. We use QPD theory to enrich the internal physical interpretation of the MF model, and point out that the fractional order factor is related to the concentration of the quasi-point defects. For $Cu_{46}Zr_{47}Al_7$ MG, the structure is in a frozen state below T_g, thus the concentration of quasi-point defects remains almost constant and the atomic mobility is limited. Above T_g, a large number of frozen atoms are activated, and the concentration of quasi-point defects increases with the increase of temperature, resulting in a significant increase of the parameter χ. In this way, through responsive combination of several well-known mechanical models, we provide a physics-motivated fractional-order description of the viscoelastic deformation in amorphous solid. It further sheds light on constructing a quantitative relationship between property and heterogeneous structure of amorphous materials.

CRediT authorship contribution statement

F. Zhu: Conceptualization, Data curation, Formal analysis, Investigation, Methodology, Writing – original draft, Writing – review & editing. **G.H. Xing:** Data curation, Formal analysis, Investigation, Methodology, Writing – original draft, Writing – review & editing. **G. J. Lyu:** Conceptualization, Formal analysis, Methodology, Writing – original draft, Writing – review & editing. **L.T. Zhang:** Formal analysis, Investigation, Writing – original draft, Writing – review & editing. **Yun-Jiang Wang:** Formal analysis, Project administration, Resources, Funding acquisition, Methodology, Writing – original draft, Writing – review & editing. **Y. Yang:** Investigation, Methodology, Writing – review & editing. **J.M. Pelletier:** Conceptualization, Data curation, Formal analysis, Investigation, Methodology,

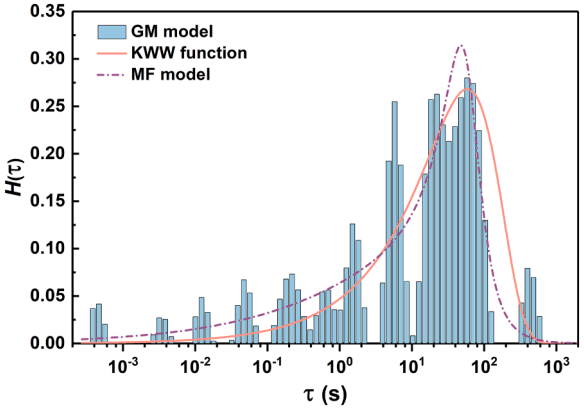

Fig. 15. The relaxation time distribution of different theoretical models, where the histogram corresponds to the GM model, the solid line corresponds to KWW function, and the dotted line corresponds to MF model.

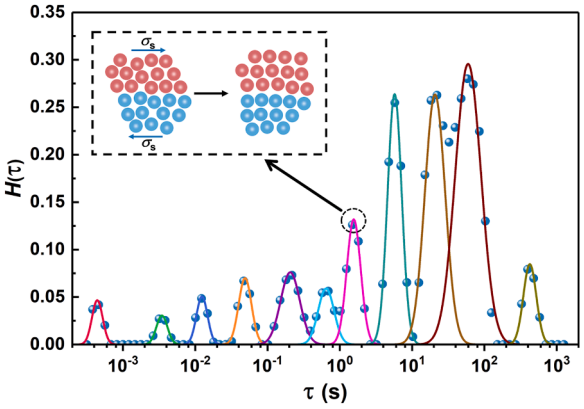

Fig. 16. Multi-peak fitting of the relaxation time. Each peak is in the log-normal form. The peak values are corresponding to specific STZs with different size and, thus, different nature of kinetics, as shown in the illustration.

Writing – original draft, Writing – review & editing. **J.C. Qiao:** Conceptualization, Formal analysis, Project administration, Resources, Funding acquisition, Methodology, Supervision, Writing – original draft, Writing – review & editing.

Declaration of Competing Interest

The authors declare that they have no known competing financial interests or personal relationships that could have appeared to influence the work reported in this paper.

Data availability

Data will be made available on request.

Acknowledgements

This work is supported by the National Natural Science Foundation of China (NSFC, Grant Nos. 51971178 and 52271153), the Fundamental Research Funds for the Central Universities (Grant No. D5000220034), Natural Science Basic Research Plan for Distinguished Young Scholars in Shaanxi Province (Grant No. 2021JC-12). Yun-Jiang Wang was financially supported by NSFC (Grant No. 12072344) and the Youth Innovation Promotion Association of the Chinese Academy of Sciences.

References

Apitz, D., Johansen, P.M., 2005. Limitations of the stretched exponential function for describing dynamics in disordered solid materials. J. Appl. Phys. 97, 063507.
Argon, A.S., 1979. Plastic deformation in metallic glasses. Acta Metallurgica 27, 47–58.

Argon, A.S., Shi, L.T., 1983. Development of visco-plastic deformation in metallic glasses. Acta Metallurgica 31, 499–507.
Arikoglu, A., 2014. A new fractional derivative model for linearly viscoelastic materials and parameter identification via genetic algorithms. Rheol. Acta 53, 219–233.
Ashby, M.F., Greer, A.L., 2006. Metallic glasses as structural materials. Scr. Mater. 54, 321–326.
Bagley, R.L., Torvik, P.J., 1983. A theoretical basis for the application of fractional calculus to viscoelasticity. J. Rheol. (N Y N Y) 27, 201–210.
Bergeret, A., Agbossou, A., Alberola, N., Cassagnau, P., Sarraf, T., 1992. Micromechanical properties of random copolymers of styrene with methacrylic acid. experimental and theoretical approaches. Eur. Polym. J. 28, 1201–1218.
Bergman, R., 2000. General susceptibility functions for relaxations in disordered systems. J. Appl. Phys. 88, 1356–1365.
Berthier, L., 2011. Dynamic heterogeneity in amorphous materials. Physics (College Park Md) 4, 42.
Berthier, L., Biroli, G., 2011. Theoretical perspective on the glass transition and amorphous materials. Rev. Mod. Phys. 83, 587–645.
Blair, G.W.S., Veinoglou, B.C., 1944. A study of the firmness of soft materials based on Nutting's equation. J. Sci. Instrum. 21, 149.
Bonfanti, A., Kaplan, J.L., Charras, G., Kabla, A., 2020. Fractional viscoelastic models for power-law materials. Soft Matter 16, 6002–6020.
Caputo, M., Mainardi, F., 1971. A new dissipation model based on memory mechanism. Pure Appl. Geophys. 91, 134–147.
Cavaillé, J.Y., Perez, J., Johari, G.P., 1991. A comparison of a point defects theory with mechanical relaxations in polymers. J. Non Cryst. Solids 131-133, 935–941.
Chen, Y., Dai, L.H., 2016. Nature of crack-tip plastic zone in metallic glasses. Int. J. Plasticity 77, 54–74.
Cheng, Y.T., Hao, Q., Pelletier, J.M., Pineda, E., Qiao, J.C., 2021. Modelling and physical analysis of the high-temperature rheological behavior of a metallic glass. Int. J. Plasticity 146, 103107.
Cui, B., Yang, J., Qiao, J., Jiang, M., Dai, L., Wang, Y.-J., Zaccone, A., 2017. Atomic theory of viscoelastic response and memory effects in metallic glasses. Phys. Rev. B 96, 094203.
Debye, P.J.W., 1929. Polar Molecules. Dover Publications.
Duan, Y.J., Zhang, L.T., Qiao, J.C., Wang, Y.J., Yang, Y., Wada, T., Kato, H., Pelletier, J.M., Pineda, E., Crespo, D., 2022. Intrinsic correlation between the fraction of liquidlike zones and the β relaxation in high-entropy metallic glasses. Phys. Rev. Lett. 129, 175501.
Egami, T., 2011. Atomic level stresses. Prog. Mater. Sci. 56, 637–653.
Failla, G., Zingales, M., 2020. Advanced materials modelling via fractional calculus: challenges and perspectives. Philosophical Trans. Royal Society A: Mathe., Phys. Engi. Sci. 378, 20200050.
Falk, M.L., Langer, J.S., 1998. Dynamics of viscoplastic deformation in amorphous solids. Phys. Rev. E 57, 7192–7205.
Fang, C.Q., Sun, H.Y., Gu, J.P., 2015. Application of fractional calculus methods to viscoelastic response of amorphous shape memory polymers. J. Mechan. 31, 427–432.
Friedrich, C., 1991. Relaxation and retardation functions of the Maxwell model with fractional derivatives. Rheol. Acta 30, 151–158.
Fu, X., Wang, G., Wu, Y., Song, W., Shek, C.H., Zhang, Y., Shen, J., Ritchie, R.O., 2020. Compressive ductility and fracture resistance in CuZr-based shape-memory metallic-glass composites. Int. J. Plasticity 128, 102687.
Gao, Y., Bei, H., 2016. Strength statistics of single crystals and metallic glasses under small stressed volumes. Prog. Mater. Sci. 82, 118–150.
Gloeckle, W.G., Nonnenmacher, T.F., 1991. Fractional integral operators and Fox functions in the theory of viscoelasticity. Macromolecules 24, 6426–6434.
Gorenflo, R., Mainardi, F., 1997. Fractional Calculus. In: Carpinteri, A., Mainardi, F. (Eds.), Fractals and Fractional Calculus in Continuum Mechanics. Springer Vienna, Vienna, pp. 223–276.
Hao, Q., Lyu, G.J., Pineda, E., Pelletier, J.M., Wang, Y.J., Yang, Y., Qiao, J.C., 2022. A hierarchically correlated flow defect model for metallic glass: universal understanding of stress relaxation and creep. Int. J. Plasticity 154, 103288.
Harmon, J.S., Demetriou, M.D., Johnson, W.L., Samwer, K., 2007. Anelastic to plastic transition in metallic glass-forming liquids. Phys. Rev. Lett. 99, 135502.
Heymans, N., 1996. Hierarchical models for viscoelasticity: dynamic behaviour in the linear range. Rheol. Acta 35, 508–519.
Jiang, F., Zhang, Z.B., He, L., Sun, J., Zhang, H., Zhang, Z.F., 2006. The effect of primary crystallizing phases on mechanical properties of $Cu_{46}Zr_{47}Al_7$ bulk metallic glass composites. J. Mater. Res. 21, 2638–2645.
Jiang, S.S., Gan, K.F., Huang, Y.J., Xue, P., Ning, Z.L., Sun, J.F., Ngan, A.H.W., 2020. Stochastic deformation and shear transformation zones of the glassy matrix in CuZr-based metallic-glass composites. Int. J. Plasticity 125, 52–62.
Jiao, W., Wen, P., Peng, H.L., Bai, H.Y., Sun, B.A., Wang, W.H., 2013. Evolution of structural and dynamic heterogeneities and activation energy distribution of deformation units in metallic glass. Appl. Phys. Lett. 102, 101903.
Ju, J.D., Atzmon, M., 2014. A comprehensive atomistic analysis of the experimental dynamic-mechanical response of a metallic glass. Acta Mater. 74, 183–188.
Ju, J.D., Jang, D., Nwankpa, A., Atzmon, M., 2011. An atomically quantized hierarchy of shear transformation zones in a metallic glass. J. Appl. Phys. 109, 053522.
Ke, H.B., Zeng, J.F., Liu, C.T., Yang, Y., 2014. Structure heterogeneity in metallic glass: modeling and experiment. J. Mater. Sci. Technol. 30, 560–565.
Kosiba, K., Şopu, D., Scudino, S., Zhang, L., Bednarcik, J., Pauly, S., 2019. Modulating heterogeneity and plasticity in bulk metallic glasses: role of interfaces on shear banding. Int. J. Plasticity 119, 156–170.
Lei, T.J., DaCosta, L.R., Liu, M., Shen, J., Sun, Y.H., Wang, W.H., Atzmon, M., 2020. Composition dependence of metallic glass plasticity and its prediction from anelastic relaxation – A shear transformation zone analysis. Acta Mater. 195, 81–86.
Li, W., Gao, Y., Bei, H., 2015. On the correlation between microscopic structural heterogeneity and embrittlement behavior in metallic glasses. Sci. Rep. 5, 14786.
Lindsey, C.P., Patterson, G.D., 1980. Detailed comparison of the Williams–Watts and Cole–Davidson functions. J. Chem. Phys. 73, 3348–3357.
Liu, M.N., Hao, Q., Pineda, E., Qiao, J.C., 2022. Evolution of the distribution of flow units of a metallic glass under cyclic loading. J. Alloys Compd. 916, 165479.
Liu, Y.H., Wang, D., Nakajima, K., Zhang, W., Hirata, A., Nishi, T., Inoue, A., Chen, M.W., 2011. Characterization of nanoscale mechanical heterogeneity in a metallic glass by dynamic force microscopy. Phys. Rev. Lett. 106, 125504.
Lukichev, A., 2019. Physical meaning of the stretched exponential Kohlrausch function. Phys. Lett. A 383, 2983–2987.
Mangion, M.B.M., Cavaillé, J.Y., Perez, J., 1992. A molecular theory for the sub-tg plastic mechanical response of amorphous polymers. Philos. Magazine A 66, 773–796.
Menard, K.P., Menard, N.R., 2020. Dynamic Mechanical Analysis. CRC Press.
Metzler, R., Schick, W., Kilian, H.G., Nonnenmacher, T.F., 1995. Relaxation in filled polymers: a fractional calculus approach. J Chem Phys 103, 7180–7186.
Nadzharyan, T.A., Kostrov, S.A., Stepanov, G.V., Kramarenko, E.Y., 2018. Fractional rheological models of dynamic mechanical behavior of magnetoactive elastomers in magnetic fields. PolymerPolymer (Guildf) 142, 316–329.
Nutting, P.G., 1921. A new general law of deformation. J. Franklin. Inst. 191, 679–685.
Palade, L.-I., Verney, V., Attané, P., 1996. A modified fractional model to describe the entire viscoelastic behavior of polybutadienes from flow to glassy regime. Rheol. Acta 35, 265–273.
Pelletier, J.M., Van de Moortèle, B., Lu, I.R., 2002. Viscoelasticity and viscosity of Pd–Ni–Cu–P bulk metallic glasses. Mater. Sci. Eng.: A 336, 190–195.
Perez, J., 1990. Quasi-punctual defects in vitreous solids and liquid-glass transition. Solid State Ionics 39, 69–79.
Perez, J., Cavaille, J.Y., Etienne, S., Fouquet, F., Guyot, F., 1983. Frottement intérieur dans les solides vitreux vers la transition vitreuse. Ann. Phys. 8, 417–467.
Pritz, T., 2003. Five-parameter fractional derivative model for polymeric damping materials. J. Sound Vib. 265, 935–952.
Qiao, J.C., Feng, S.D., Pelletier, J.M., Crespo, D., Pineda, E., Yao, Y., 2017. Physical aging effects on the dynamic relaxation behavior and mechanical properties of Cu46Zr46Al8 metallic glass. J. Alloys Compd. 726, 195–200.
Qiao, J.C., Pelletier, J.M., 2014a. Dynamic mechanical relaxation in bulk metallic glasses: a review. J. Mater. Sci. Technol. 30, 523–545.
Qiao, J.C., Pelletier, J.M., 2014b. Dynamic universal characteristic of the main (α) relaxation in bulk metallic glasses. J. Alloys Compd. 589, 263–270.
Qiao, J.C., Wang, Q., Pelletier, J.M., Kato, H., Casalini, R., Crespo, D., Pineda, E., Yao, Y., Yang, Y., 2019. Structural heterogeneities and mechanical behavior of amorphous alloys. Prog. Mater. Sci. 104, 250–329.
Qiao, J.C., Yao, Y., Pelletier, J.M., Keer, L.M., 2016. Understanding of micro-alloying on plasticity in $Cu_{46}Zr_{47-x}Al_7Dy_x$ ($0 \leq x \leq 8$) bulk metallic glasses under compression: based on mechanical relaxations and theoretical analysis. Int. J. Plasticity 82, 62–75.

Qiao, J.C., Zhang, L.T., Tong, Y., Lyu, G.J., Hao, Q., Tao, K., 2022. Mechancial properties of amorphous alloys: in the framework of the microstructure heterogeneity. Adv. Mech. 52, 117–152.
Reyes-Melo, E., Martínez-Vega, J., Guerrero-Salazar, C., Ortiz-Méndez, U., 2004. On the modeling of the dynamic-elastic modulus for polymer materials under isochronal conditions. J. Appl. Polym. Sci. 94, 657–670.
Rinaldi, R., Gaertner, R., Chazeau, L., Gauthier, C., 2011. Modelling of the mechanical behaviour of amorphous glassy polymer based on the Quasi point defect theory—part I: uniaxial validation on polycarbonate. Int. J. Non Linear Mech. 46, 496–506.
Schiessel, H., Metzler, R., Blumen, A., Nonnenmacher, T.F., 1995. Generalized viscoelastic models: their fractional equations with solutions. J. Phys. A Math. Gen. 28, 6567–6584.
Serra-Aguila, A., Puigoriol-Forcada, J.M., Reyes, G., Menacho, J., 2019. Viscoelastic models revisited: characteristics and interconversion formulas for generalized Kelvin–Voigt and Maxwell models. Acta Mechanica Sinica 35, 1191–1209.
Sha, Z.-D., Branicio, P.S., Lee, H.P., Tay, T.E., 2017. Strong and ductile nanolaminate composites combining metallic glasses and nanoglasses. Int. J. Plasticity 90, 231–241.
Sharma, R., Cherayil, B.J., 2010. Polymer melt dynamics: microscopic roots of fractional viscoelasticity. Phys. Rev. E 81, 021804.
Tao, K., Li, F.C., Liu, Y.H., Pineda, E., Song, K.K., Qiao, J.C., 2022. Unraveling the microstructural heterogeneity and plasticity of $Zr_{50}Cu_{40}Al_{10}$ bulk metallic glass by nanoindentation. Int. J. Plasticity 154, 103305.
Tao, K., Qiao, J.C., Zhang, L., Pelletier, J.M., 2021. Dynamic mechanical response of ZrCu-based bulk metallic glasses. Int. J. Mechan. Sci. 211, 106770.
Tschoegl, N.W. 1989. The phenomenological theory of linear viscoelastic behavior: An Introduction. Springer Berlin, Heidelberg, 1–34.
Turnbull, D., Cohen, M.H., 1970. On the free-volume model of the liquid-glass transition. J. Chem. Phys. 52, 3038–3041.
Van Loock, F., Brassart, L., Pardoen, T., 2021. Implementation and calibration of a mesoscale model for amorphous plasticity based on shear transformation dynamics. Int. J. Plasticity 145, 103079.
Wagner, H., Bedorf, D., Küchemann, S., Schwabe, M., Zhang, B., Arnold, W., Samwer, K., 2011. Local elastic properties of a metallic glass. Nat. Mater. 10, 439–442.
Wang, B., Kari, L., 2020. A visco-elastic-plastic constitutive model of isotropic magneto-sensitive rubber with amplitude, frequency and magnetic dependency. Int. J. Plasticity 132, 102756.
Wang, W.H., 2012. The elastic properties, elastic models and elastic perspectives of metallic glasses. Prog. Mater. Sci. 57, 487–656.
Wang, W.H., 2019. Dynamic relaxations and relaxation-property relationships in metallic glasses. Prog. Mater. Sci. 106, 100561.
Wang, Z., Sun, B.A., Bai, H.Y., Wang, W.H., 2014. Evolution of hidden localized flow during glass-to-liquid transition in metallic glass. Nat. Commun. 5, 5823.
Wang, Z., Wang, W.H., 2018. Flow units as dynamic defects in metallic glassy materials. Natl. Sci. Rev. 6, 304–323.
Wang, Z., Yu, H.B., Wen, P., Bai, H.Y., Wang, W.H., 2011. Pronounced slow β-relaxation in La-based bulk metallic glasses. J. Phys.: Condensed Matter 23, 142202.
Xie, Z., Zhang, Y., Yang, Y., Chen, X., Tao, P., 2010. Effects of rare-earth elements on the glass-forming ability and mechanical properties of $Cu_{46}Zr_{47-x}Al_7M_x$(M = Ce, Pr, Tb, and Gd) bulk metallic glasses. Rare Metals 29, 444–450.
Xu, D., Duan, G., Johnson, W.L., 2004. Unusual Glass-Forming Ability of Bulk Amorphous Alloys Based on Ordinary Metal Copper. Phys. Rev. Lett. 92, 245504.
Xu, Z.R., Qiao, J.C., Wang, J., Pineda, E., Crespo, D., 2022. Comprehensive insights into the thermal and mechanical effects of metallic glasses via creep. J. Mater.Sci. Technol. 99, 39–47.
Yang, Y., Zeng, J.F., Volland, A., Blandin, J.J., Gravier, S., Liu, C.T., 2012. Fractal growth of the dense-packing phase in annealed metallic glass imaged by high-resolution atomic force microscopy. Acta Mater. 60, 5260–5272.
Yao, Z.F., Qiao, J.C., Pelletier, J.M., Yao, Y., 2017. Characterization and modeling of dynamic relaxation of a Zr-based bulk metallic glass. J. Alloys Compd. 690, 212–220.
Yu, H.B., Shen, X., Wang, Z., Gu, L., Wang, W.H., Bai, H.Y., 2012. Tensile plasticity in metallic glasses with pronounced β relaxations. Phys. Rev. Lett. 108, 015504.
Zhai, W., Wang, C.H., Qiao, J.C., Pelletier, J.M., Dai, F.P., Wei, B., 2018. Distinctive slow β relaxation and structural heterogeneity in (LaCe)-based metallic glass. J. Alloys Compd. 742, 536–541.
Zhang, L.T., Duan, Y.J., Wada, T., Kato, H., Pelletier, J.M., Crespo, D., Pineda, E., Qiao, J.C., 2021. Dynamic mechanical relaxation behavior of $Zr_{35}Hf_{17.5}Ti_{5.5}Al_{12.5}Co_{7.5}Ni_{12}Cu_{10}$ high entropy bulk metallic glass. J. Mater. Sci. Technol. 83, 248–255.
Zhang, L.T., Wang, Y.J., Pineda, E., Yang, Y., Qiao, J.C., 2022. Achieving structural rejuvenation in metallic glass by modulating β relaxation intensity via easy-to-operate mechanical cycling. Int. J. Plasticity 157, 103402.
Zhang, M., Chen, Y., Li, W., 2019. On the origin of softening in the plastic deformation of metallic glasses. Int. J. Plasticity 116, 24–38.